Available online at www.sciencedirect.com
ScienceDirect
Ceramics International 38S (2012) S617–S621
CERAMICS INTERNATIONAL
www.elsevier.com/locate/ceramint

# Characteristics of Ti-doped ITO films grown by DC magnetron sputtering

Sung Mook Chung [a,*], Jae Heon Shin [a], Woo-Seok Cheong [a], Chi-Sun Hwang [a], Kyoung Ik Cho [a], Young Jin Kim [b]

[a] Convergence Components & Materials Research Laboratory, Electronics and Telecommunications Research Institute, Deajeon 305-700, Republic of Korea
[b] Department of Materials Science and Engineering, Kyonggi University, Suwon 443-760, Republic of Korea

Available online 27 May 2011

**Abstract**

We have investigated the effects of Ti doping on the structural, optical, and electrical properties of indium tin oxide (ITO) thin films prepared by direct-current (DC) sputtering at room temperature. It is observed that the Ti doping changes the microstructure of the ITO films from amorphous to polycrystalline improving the electrical properties. The optimized ITO:Ti thin film after annealing shows a carrier concentration of $6.24 \times 10^{20}$ cm$^{-3}$, a mobility of 34 cm$^2$/V s, and a resistivity of $2.3 \times 10^{-4}$ Ω cm. The ITO:Ti film also shows a better thermal stability up to 450 °C.


*Keywords:* C. Electrical properties; C. Thermal properties; D. $TiO_2$; Sputtering

## 1. Introduction

The high electrical conductivity combined with high transmission in the visible spectral range of ITO films has been widely utilized as an essential part of many optoelectronic devices such as plasma display panels (PDPs), liquid crystal displays (LCDs), light emitting diodes (LEDs), touch sensitive over layers, and solar cells [1,2]. ITO thin film is a highly degenerate n-type semiconductor which has a low electrical resistivity of $2–4 \times 10^{-4}$ Ω cm. The degeneracy is caused by both the intentional Sn doping and the inherent oxygen vacancies, which create donor levels in the energy band gap [3]. ITO films can be prepared by various techniques, such as chemical vapor deposition (CVD), thermal evaporation, DC and radio-frequency (RF) magnetron sputtering techniques, spray pyrolysis, pulsed laser deposition, and sol–gel method [1–4]. The magnetron sputtering techniques are most compatible with the integrated circuit processing, which can continuously produce large area ITO films at a lower processing temperature [3,4]. In the case of the magnetron sputtering techniques, the precise controls of oxygen flow and target composition ratio are very important to the deposition of ITO films due to the oxidation state and the amount of Sn dopant [5]. Moreover, carrier density may also be modified by the post-annealing process by means of changes in the Sn-activation state [6]. Many studies aimed at improving the electrical and optical properties by optimizing the above deposition and anneal conditions are frequently conducted [5–7]. However, very few studies report on the effects of additional dopant such as Zn, Ce, and Ti on the electrical and optical properties of ITO films [8].

In this paper, we report on the characteristics of Ti-doped ITO (ITO:Ti) films prepared by the DC magnetron sputtering. ITO and ITO:Ti films have been grown on glass substrates by a DC sputtering system at room temperature and post-annealed at 250 °C. From the X-ray diffraction (XRD) measurements, we observe that the Ti doping changes the microstructure of the ITO films from amorphous to polycrystalline resulting in improved electrical properties.

## 2. Experimental

ITO films were grown on alkali-free glass (Corning 1737) substrates using a DC magnetron sputtering system along with working gases Ar and $O_2$ without substrate heating. An ITO ceramic target made by sintering a mixture of 98 wt.% indium oxide ($In_2O_3$) and 2 wt.% of tin oxide ($SnO_2$) was used in the sputtering process, after which, ITO:Ti films were produced by

* Corresponding author. Tel.: +82 42 860 1063; fax: +82 42 860 5202.
*E-mail address:* smchung@etri.re.kr (S.M. Chung).

0272-8842/$36.00 
doi:10.1016/j.ceramint.2011.05.110

co-sputtering with the ITO target and a $TiO_x$ target. The $O_2$/($Ar + O_2$) ratio and working pressure were about 1% and 5 mTorr, at room temperature, respectively. The Ti atomic ratio in the ITO:Ti films is controlled by the sputter power ratio between the ITO and $TiO_x$ targets. The heat treatments of the films were carried out in a box furnace for 2 h at 250 °C in vacuum condition.

A scanning electron microscope (SEM, FEI Sirion400, Netherland) with an energy dispersive spectrometer (EDS) was used to analyze the surface morphology, the Ti atomic ratio, and film thickness. The structural changes were analyzed by using a $2\theta$ X-ray diffraction (XRD, Rigaku D/max-RC300, Japan). Hall-effect measurements (Accent HL5500PC, USA) were carried out in the van-der-Pauw configuration at room temperature. The room-temperature transmittance measurements were performed using an ultraviolet–visible (UV–VIS) spectrophotometer (Hitachi U-3501, Japan).

## 3. Results and discussion

The XRD patterns of ITO and ITO:Ti(2.5%) films with/without post-annealing are presented in Fig. 1(a) and (b). The ITO film post-annealed at 250 °C shows a polycrystalline structure. It is well known that the ITO films prepared with low oxygen proportion achieve a crystalline cubic structure after heating at 200 °C or above with diffraction peaks corresponding to (2 1 1), (2 2 2), and (4 0 0) directions [5]. In the case of ITO:Ti films, they show stronger crystalline properties as shown in Fig. 1(b). Even the as-deposited ITO:Ti film shows a clear crystalline phase in Fig. 1(b). Yang et al. reported similar crystalline properties with some amount of amorphous phase in the as-deposited ITO:Ti films [9]. However, the clear crystalline property with no amorphous phase in our as-deposited ITO:Ti films is observed for the first time. In the case of ITO:Ce, Kang et al. reported the reduction of grain growth during the post-anneal process resulting in the amorphous phase even after the post-anneal process [10]. They attributed the inhibition of grain growth in the ITO:Ce films to the larger ionic radius of $Ce^{4+}$ (0.103 nm) than that of $In^{3+}$ (0.092 nm) or $Sn^{4+}$ (0.071 nm) [10]. The ionic radius of $Ti^{4+}$ is about 0.068 nm [9]. Therefore, we hypothesize that the strong crystalline growth in our ITO:Ti films may be related to the small ionic radius of the $Ti^{4+}$. The difference in the crystalline property between this work and the work of Yang et al. may be originated from the different target and deposition conditions, such as the oxygen ratio. Fig. 1(b) shows that the ITO:Ti film with post-annealing has a more observable crystalline characteristic than the as-deposited films. The grain sizes are calculated from the line broadening of the (2 2 2) diffraction line according to the Scherrer equation [9]. The calculated grain sizes of the ITO:Ti films before and after annealing are 57 nm and 97 nm, respectively.

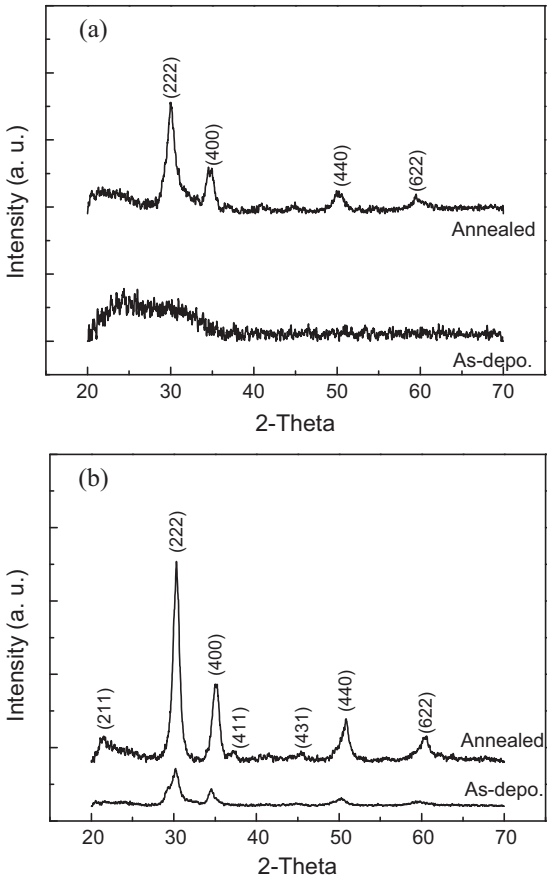


Fig. 1. XRD patterns of ITO and ITO:Ti(2.5%) thin films grown on glass substrates: (a) ITO and (b) ITO:Ti. The sputtering processes were conducted at room temperature with a working pressure and a gas flow ratio ($O_2$/($Ar + O_2$)) of 5 mTorr and 1%, respectively. The post-annealing was done at 250 °C for 2 h at vacuum condition.

The results of Hall transport measurements of all the ITO films are presented in Table 1. All the films have a similar thicknesses of about 130–140 nm confirmed by SEM. Table 1 shows that the mobility and the resistivity have a maximum of 34 $cm^2$/V s and a minimum of $2.3 \times 10^{-4}$ Ω cm, respectively, at the Ti atomic ratio of 2.5%. The higher mobility and the lower carrier concentration of the ITO:Ti(2.5%) film comparing to those of the ITO film may be related to the stronger crystallization property as shown in Fig. 1. However, the mobility and the carrier concentration decreases and increases, respectively, as the Ti ratio increases above 2.5%. Yang et al. reported that a high number of Ti atoms may play a role of ionized impurity scattering, resulting in the decrease of the mobility with the Ti atoms [9]. The ITO:Ti(2.5%) film has about 20% lower resistivity than the ITO film as shown in Table 1.

Fig. 2 shows transmittance spectra of ITO and ITO:Ti(2.5%) films after post-annealing measured at room temperature by

Table 1
Electrical properties of ITO and ITO:Ti films.

| Ti ratio (atomic %) | Resistivity (Ω cm) | Hall mobility ($cm^2$/V s) | Carrier concentration ($cm^{-3}$) |
|---|---|---|---|
| 0 | $2.84 \times 10^{-4}$ | 26.9 | $8.24 \times 10^{20}$ |
| 2.5 | $2.3 \times 10^{-4}$ | 34.0 | $6.24 \times 10^{20}$ |
| 5 | $2.6 \times 10^{-4}$ | 27.4 | $7.74 \times 10^{20}$ |
| 7.5 | $3.05 \times 10^{-4}$ | 26.6 | $7.99 \times 10^{20}$ |
| 10 | $3.25 \times 10^{-4}$ | 24.9 | $8.12 \times 10^{20}$ |
| 12.5 | $4.0 \times 10^{-4}$ | 20.8 | $8.14 \times 10^{20}$ |
| 15 | $4.3 \times 10^{-4}$ | 19.1 | $10.52 \times 10^{20}$ |

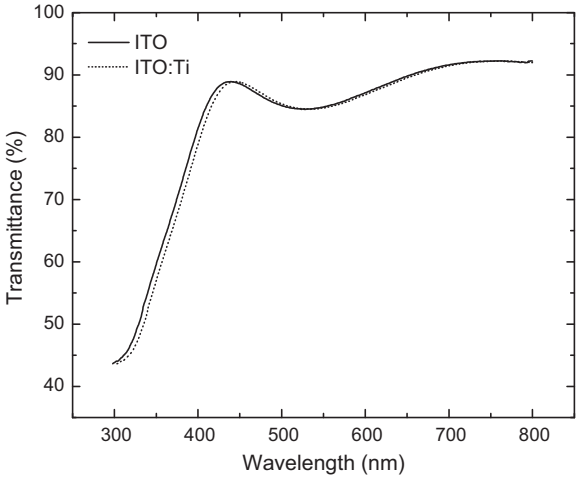


Fig. 2. Transmittance spectra of the post-annealed ITO and ITO:Ti(2.5%) thin films.

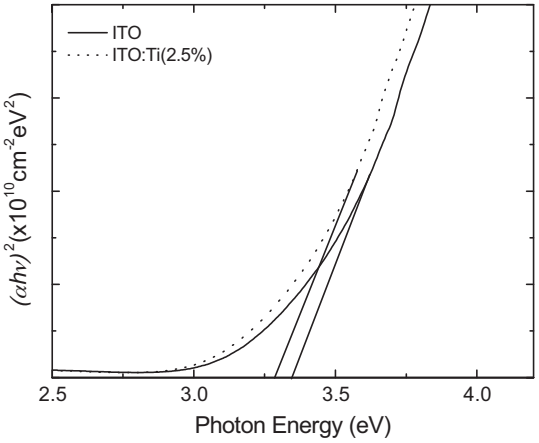


Fig. 3. Band-gap determination of the post-annealed ITO and ITO:Ti(2.5%) thin films.

using an UV–VIS spectrometer. The average transmittance in the visible wavelength (at 550 nm) region is above 84% for both films. In Fig. 2, the absorption edge of the ITO:Ti(2.5%) film shifts toward the red region, which was also observed by Yang et al. at annealing temperatures from 300 °C to 450 °C [9]. It is known that the band gap of ITO film increases with the increase of carrier concentration by the Burstein–Moss (BM) effect, i.e. screening of the lowest conduction band states [11]. The red shift of the band gap of our ITO:Ti film might also be explained by the BM effect since our ITO:Ti film has lower carrier concentration than the ITO film. To measure the energy band gap from the transmittance spectra, one uses the relation,

$$\alpha h\nu = A(h\nu - E_g)^n \quad (1)$$

where $h\nu$ is the photon energy, $\alpha$ the absorption coefficient, $E_g$ the band-gap, $A$ the proportional coefficient, and $n = 1/2$ for direct band-gap material [12]. To measure the energy band-gap from the absorption spectra, a graph of $[(\alpha - \alpha_1)h\nu]^{1/n}$ versus $h\nu$ was plotted as shown in Fig. 3, where $\alpha_1$ is the minimum value of the absorption coefficient [12]. The absorption coeffi-

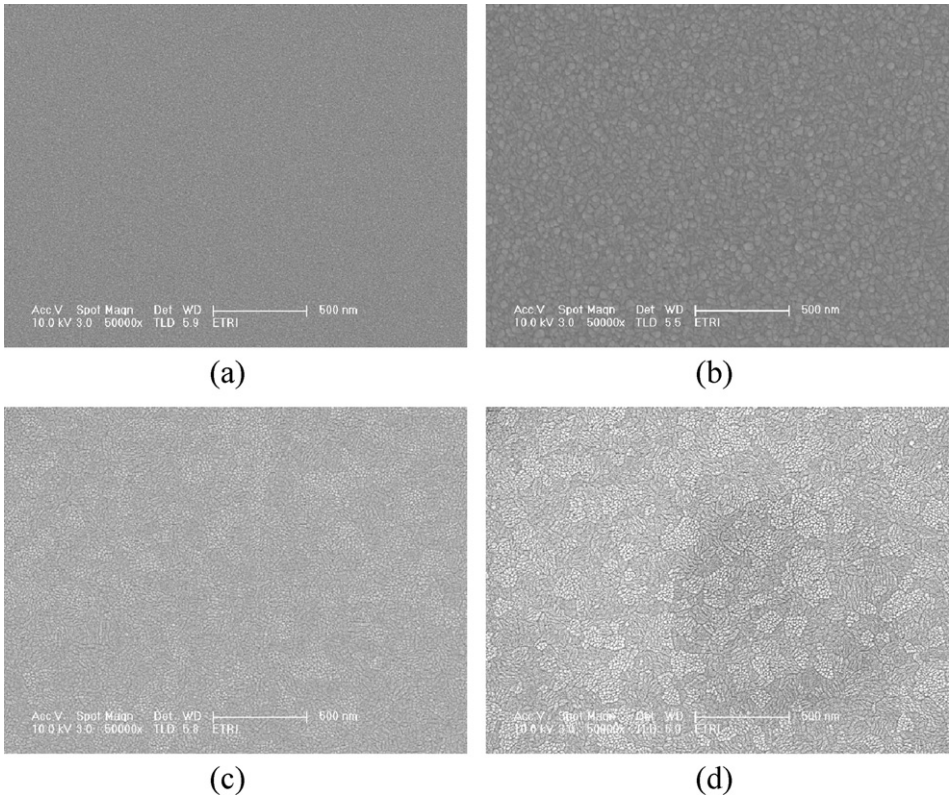


Fig. 4. SEM images of the ITO and ITO:Ti(2.5%) thin films: (a) as-deposited ITO, (b) annealed ITO, (c) as-deposited ITO:Ti(2.5%), and (d) annealed ITO:Ti(2.5%).

cient $\alpha$ was calculated from the transmittance curve with corrections for multiple reflections [12]. The energy band-gap obtained from the extrapolation of the straight lines in Fig. 3 are 3.34 and 3.27 eV for ITO and ITO:Ti(2.5%), respectively.

Fig. 4 shows the SEM images of the ITO and ITO:Ti(2.5%) films: (a) as-deposited ITO, (b) annealed ITO, (c) as-deposited ITO:Ti, and (d) annealed ITO:Ti. In Fig. 4(a), the as-deposited ITO film shows quite a smooth surface indicating the amorphous phase without any grain structures. On the contrary, in Fig. 4(c), the as-deposited ITO:Ti(2.5%) film shows a grain structure indicating the nanocrystalline property. Therefore, it is concluded that the SEM morphology data coincides with the XRD data. In Fig. 4(b) and (d), the grain size increases with heat treatment as predicted from the XRD data. No aggregated particles such as Ti or $TiO_2$ is observed in the ITO:Ti film.

Fig. 5 shows the measured electrical properties after additional substrate heating process in atmosphere condition at 1 h. It is known that the electrical properties of ITO film are affected by the change of crystallinity, stoichiometry, and the density of oxygen vacancy during substrate heating in atmosphere condition [13]. In Fig. 5(a), The dramatic increase of the resistivity, i.e. the decrease of the carrier density, of the ITO and ITO:Ti(2.5%) films above 350 °C might be originated from the decrease of both the oxygen vacancies and the Sn dopants [13]. As shown in Fig. 5(a) and (b), the ITO:Ti film shows more stable and uniform electrical properties than the ITO film during the high temperature heating process, which might be due to the more strong crystallinity property of the ITO:Ti film. However, further studies are needed to resolve the exact mechanism of the thermal stability of the ITO:Ti film.

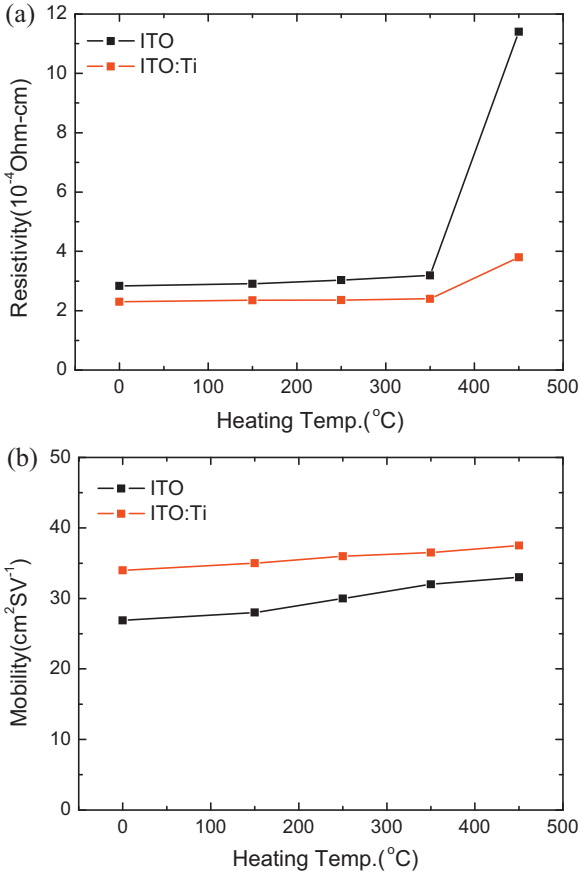


Fig. 5. Electrical properties vs. post-heating temperature: (a) electrical resistivity and (b) mobility. The heating processes were conducted in atmosphere condition for 1 h.

## 4. Conclusions

ITO and ITO:Ti thin films have been grown on glass substrates by a DC sputtering system at room temperature and post-annealed for 2 h at 250 °C in vacuum condition. The microstructure change from amorphous to polycrystalline structure for the as-deposited ITO:Ti films was confirmed by XRD and SEM measurements. The optimized ITO:Ti thin film shows a carrier concentration of $6.24 \times 10^{20}$ cm$^{-3}$, a mobility of 34 cm$^2$/V s, and a resistivity of $2.3 \times 10^{-4}$ Ω cm at the Ti atomic ratio of 2.5%. The ITO:Ti film also shows a better thermal stability, which is thought to be due to the polycrystalline structure. Those results indicate that the ITO:Ti thin films with good thermal stability can be applied to various opto-electronic devices.

## Acknowledgement

This work was supported by the IT R&D program of MKE/KEIT [2006-S079-05, Smart window with transparent electronic devices].

## References

[1] A. Solieman, M.A. Aegerter, Modeling of optical and electrical proeprties of $In_2O_3$:Sn coatings made by varous techniques, Thin Solid Films 502 (2006) 205–211.
[2] J.H. Shin, J.S. Lee, C.S. Hwang, S.H. KoPark, W.S. Cheong, M.K. Ryu, C.W. Byun, J.I. Lee, H.Y. Chu, Light effects on the bias stability of transparent ZnO thin film transistors, ETRI Journal 31 (2009) 62–64.
[3] H.-C. Lee, O.O. Park, Behaviors of carrier concentrations and mobilities in indium-tin oxide thin films by DC magnetron sputtering at various oxygen flow rates, Vacuum 77 (2004) 69–77.
[4] W.-S. Cheong, J.-M. Lee, S.-H. Ko Park, S.M. Yoon, C.-W. Byun, S.H. Yang, S.M. Chung, K.I. Cho, C.-S. Hwang, Effects of interfacial dielectric layers on the electrical performance of top-gate In–Ga–Zn–oxide thin-film transistors, ETRI Journal 31 (2009) 660–666.
[5] L.R. Cruz, C. Legnani, I.G. Matoso, C.L. Ferreria, H.R. Moutinho, Influence of pressure and annealing on the microstructural and electro-optical properties of RF magnetron sputtered ITO thin films, Materials Research Bulletin 39 (2004) 993–1003.
[6] H. Han, J.W. Mayer, T.L. Alford, Band gap shift in the indium-tin-oxide films on polyethylene napthalate after thermal annealing in air, Journal of Applied Physics 100 (2006) 083715,1–083715,6.
[7] T. Minami, Present status of transparent conducting oxide thin-film development for indium-tin oxide (ITO) substitutes, Thin Solid Films 516 (2008) 5822–5828.
[8] D.-S. Liu, C.-S. Sheu, C.-T. Lee, C.-H. Lin, Thermal stability of indium tin oxide thin films co-sputtered with zinc oxide, Thin Solid Films 516 (2008) 3196–3203.
[9] C.–H. Yang, S.-C. Lee, T.-C. Lin, W.-Y. Zhuang, Opto-electronic properties of titanium-doped indium-tin-oxide films deposited by RF magnetron sputtering at room temperature, Materials Science Engineering B 134 (2006) 68–75.

[10] Y.M. Kang, S.H. Kwon, J.H. Choi, Y.J. Cho, P.K. Song, Properties of Ce-doped ITO films deposited on polymer substrate by DC magnetron sputtering, Thin Solid Films 518 (2010) 3081–3084.
[11] I. Hamberg, C.G. Granqvist, Band-gap widening in heavily Sn-doped $In_2O_3$, Physical Review B 30 (1984) 3240–3249.
[12] J. Tanc, Amorphous and Liquid Semiconductor, Plenum, New York, 1974.
[13] G.H. Guai, Q.L. Song, Z.S. Lu, C.-M. Li, Effects of multiple heat treatment cycles on structure, optical and electrical properties of indium-tin-oxide thin films, Surface & Coatings Technology 205 (2011) 2852.